Shallow water model for horizontal centrifugal casting

2012 IOP Conf. Ser.: Mater. Sci. Eng. 33 012032

(http://iopscience.iop.org/1757-899X/33/1/012032)

Shallow water model for horizontal centrifugal casting

J Boháček[1], A Kharicha[2], A Ludwig[2] and M Wu[2]

[1]Materials Center Leoben Forschung GmbH, A-8700 Leoben, Roseggerstr. 12, Austria
[2]Chair for Simulation and Modelling of Metallurgical Processes, Dept. Metallurgy, University of Leoben, 8700 Leoben, Franz-Josef-Str. 18/III, Austria

E-mail: jan.bohacek@mcl.at

Abstract. A numerical model was proposed to simulate the solidification process of an outer shell of work roll made by the horizontal centrifugal casting technique. Shallow water model was adopted to solve the 2D average flow dynamics of melt spreading and the average temperature distribution inside the centrifugal casting mould by considering the centrifugal force, Coriolis force, viscous force due to zero velocity on the mould wall, gravity, and energy transport by the flow. Additionally, a 1D sub-model was implemented to consider the heat transfer in the radial direction from the solidifying shell to the mould. The solidification front was tracked by fulfilling the Stefan condition. Radiative and convective heat losses were included from both, the free liquid surface and the outer wall of the mould. Several cases were simulated with the following assumed initial conditions: constant height of the liquid metal (10, 20, and 30 mm), uniform temperature of the free liquid surface (1755 K). The simulation results have shown that while the solidification front remained rather flat, the free surface was disturbed by waves. The amplitude of waves increased with the liquid height. Free surface waves diminished as the solidification proceeded.

1. Introduction

The horizontal spin (or centrifugal) casting process (HSC) has several advantages over the conventional gravity casting and many other casting processes. Due to a high degree of metallurgical purity, minimum of shrinkage cavities, and homogeneous microstructure with very fine crystals, the centrifugally cast products generally show superior mechanical properties such as the rupture strength, the rupture strain, and the Young modulus [1]. Two physical phenomena contribute to these outstanding features. The first one is the high centrifugal force. The solidification usually starts immediately at the moment when the liquid metal gets in first contact with the mould wall, and cloud of fine crystals nucleate near the mould region. A certain portion of them is brought back into bulk by the high centrifugal force and these free crystals serve as new nucleation sites, continue to grow in the bulk, hence fine structure is achieved throughout. Moreover, the high centrifugal force supresses the possible occurrence of shrinkage, the air gap between the mould and the solidified shell, and enhances the solidification rate. The second phenomenon is the inherent vibration, which has also a positive impact on the mechanical properties by promoting a higher solidification rate and turbulent flow.

The impact of the centrifugal force, which is determined by the product of radius and the square of angular frequency, is twofold. A too low angular frequency can cause so-called raining i.e. metal droplets can fall down from the upper part of the inside surface of the casting product [2]. On the other hand, excessive speeds usually accompanied by strong vibrations can lead to longitudinal cracks caused by the hoop stress in the initially solidified shell. Furthermore, increasing the angular

frequency promotes segregation. Therefore, the centrifugal force, together with many other process parameters like the pouring temperature, pouring rate and the mould coating etc., need the optimal control.

Quite amount of experimental studies on the centrifugal effect were performed. For example, Chirita and co-workers [3] found that the centrifugal force acts on the casting process by three separate mechanisms: the centrifugal pressure, the inherent vibration, and the fluid dynamics. First, the centrifugal pressure as one of the promoting mechanisms is naturally responsible for the elimination of the shrinkage (the gap between the mould and the shell) and the shrinkage porosity. The quality improvement could be also theoretically attributed to the shift of the phase diagram, which commonly happens in the squeeze casting. In the HSC this was however not proven. Next, the inherent vibration caused by quasi-static imbalances in the rotating system can enhance the melt mixing, which naturally leads to a higher heat transfer rate. The presence of the vibration promotes a transition from the lamellar to the fibrous morphology of the casting microstructure. The vibration was also proved to increase the eutectic volume fraction. However, a critical value of centrifugal acceleration was also found at which the grains tend to coarsen. They also reported some drop in the volume fraction and size of pores, but again a critical value of centrifugal acceleration most likely exists. Finally, the fluid dynamics plays an important role especially during the filling, when it washes newly solidified crystals out from the wall back into the melt. Here, these fragments stand for new nucleation sites and promote solidification of equiaxed crystals. The fluid dynamics also enhances mixing and solidification rate, consequently.

Only few numerical studies have been devoted to the horizontal spin casting. In the work of [4], an effort for a comprehensive description of the flow dynamics of the melt inside the horizontally rotating mould was done using the VOF model (STAR-CD). Two phases were considered, the liquid metal and the surrounding air. The time step was notably large (~0.01 s) which implies a very rough calculation. Nevertheless, the results were found to be in quite good agreement with experimental data. Zagórski and co-workers [5] used the similar VOF model to study the initial stage of mould filling during the vertical centrifugal casting of metal matrix composite reinforced with SiC. Additionally, a discrete phase model was used to track SiC particles. The problem was solved as 2D axisymmetric with swirl component of velocity and all calculations were terminated at 1 s of real time. A simple solidification model for planar front, coupled with equations for force balance on dispersed ceramic particles, was used by Raju and co-workers [6] to describe the centrifugal casting process of metal matrix composite. The flow dynamics was ignored. Segregation of particles was extensively studied with respect to heat transfer coefficient between the mould and the casting. Interesting work was done by Drenchev and co-workers [7] on macrostructure formation during centrifugal casting of particle reinforced metal matrix composites. System of PDEs was solved for particle movement, heat conduction inside the mould and casting, and the solidification considering a linear temperature profile in the mushy zone.

The aim of the current paper is to develop a mathematical model capable of simulating the main features of the flow dynamics inside a horizontally rotating mould coupled with heat transfer and solidification. We target at the entire HSC process i.e. the casting of the pure shell and the intermediate shell with the filling system included. The High Speed Steel (HSS) is used for the casting of the pure (or outer) shell, while the intermediate layer is made of the grey cast iron. The HSC duration is approximately 30 min. Due to the nature of multi-physics spanning different time scales (flow dynamics vs. solidification rate) the numerical model has to be simple and robust. In this paper, the model was tested without the filling system. For this reason, a certain height of the liquid metal (10, 20, and 30 mm) with a constant temperature of 1755 K was evenly imposed everywhere inside the mould in the beginning of each simulation.

2. Numerical model

The present work is based on a so-called shallow water model. The fundamental model theory can be found in literatures [8]-[10]. The shallow water equations were originally derived in one dimensional form as so-called Saint-Venant equations [11]. This model was implemented by the authors in the

commercial CFD package ANSYS-FLUENT. The calculation domain comprises 4 layers (Figure 1), representing the mould, the solid metal, the liquid melt and air, respectively. More details on the model settings can also be found elsewhere in [12]-[13].

2.1. Flow modelling

Flow is only necessarily solved in the layers of liquid melt and air. The solid layer is assumed to be in perfect contact with the mould, rotating with a pre-described velocity. The air flow is not of significant importance, since momentum transfer with the liquid melt is ignorable. The flow in the liquid melt layer is considered to be laminar. Therefore, a parabolic velocity profile is imposed with zero shear stress on the free surface. Due to a high angular frequency Ω (~70 rads^{-1}) of the system the liquid melt is mainly rotating with the mould; thus, the model can be defined in the rotating frame of reference, and fictitious forces (centrifugal and Coriolis forces) are included in the momentum equations as source terms. The continuity equation is defined as:

$$\frac{\partial(h\rho)}{\partial t} + \nabla \cdot \left(h\rho\vec{u}\right) = S_{m,l\to s}, \tag{1}$$

where h denotes the height of the liquid layer and $S_{m,l\to s}$ is the mass transfer from liquid to solid due to solidification. The momentum equations for x and y coordinates are defined as:

$$\begin{aligned} &\frac{D}{Dt}\left(h\rho\vec{u}\right) + \rho h\Omega^2\left(R_{in} - h - \delta\right)\nabla\left(h+\delta\right) + \rho h\left|\vec{\Omega}\right|\left(2u_y\nabla\delta + \frac{5}{2}u_y\nabla h + \frac{5}{4}h\nabla u_y\right) = \\ &-h\nabla p + h\mu\nabla^2\vec{u} - \rho h\vec{g}\left[\left(0, \sin\left(\left|\vec{\Omega}\right|t + \frac{y}{R_{in}}\right)\right) + \cos\left(\left|\vec{\Omega}\right|t + \frac{y}{R_{in}}\right)\nabla\left(h+\delta\right)\right] - 3\mu\frac{\vec{u}}{h} + F_{l\to s} \end{aligned}, \tag{2}$$

The terms on the left-hand side of equation (2) represent inertia forces, which includes centrifugal and Coriolis forces. On the right-hand side of equation (2), the first term is the force induced due to the gradient of the static pressure. The second term handles the momentum losses resulting from stress tensor but only in tangential and axial direction. The last three terms represent the gravity force, the viscous force in the radial direction due to the no-slip BC on the mould wall, and the momentum transfer from liquid to solid due to solidification, respectively.

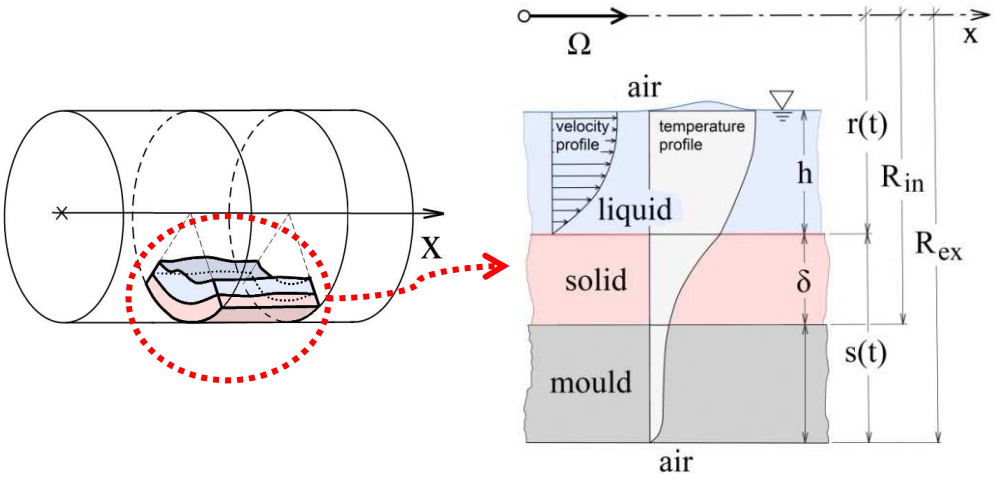

Figure 1. Schematic of a part of the horizontal centrifugal casting section.

2.2. Mould deformation and vibration

As discussed above, vibrations can strongly influence solidification and final quality of the product, consequently. Measurement of vibrations during the real HSC is a standard procedure and vibrations are always present. There are several possible origins of vibrations. One is due to large mould dimensions that the mould is in static imbalance because of the poor roundness of cylindrical surfaces. This becomes even worse during the filling, when the melt is unevenly spread inside the mould. Another reason is that temperature gradients through the thickness of the mould cause thermo-mechanical stresses and deformations. The present model treats vibrations as a time dependent perturbation of gravity as proposed in [14]. Corresponding acceleration can be defined as:

$$\overrightarrow{a_v} = \left(0, \quad \xi\cos\left(\omega t + \beta\right), \quad \xi\sin\left(\omega t + \beta\right)\right)^T, \tag{3}$$

where ξ is the amplitude of acceleration due to vibrations, ω is the angular frequency associated to vibrations, and β is the phase. The phase β specifies the position where the oscillation begins. In the model β is set constant ($\pi/2$). The angular frequency ω is set to the double of the angular frequency Ω assuming an elliptical cross section of the mould. Besides, axial deformation of the mould due to temperature gradients is also taken into account using the following sine-like axis profile:

$$\tan\theta = A\frac{\pi}{\lambda}\cdot\sin\left(\frac{\pi x}{\lambda}\right), \tag{4}$$

where A is the amplitude of bending, x is the axial coordinate, θ is the angle between the x-axis and the deformed mould centreline, and λ is the distance between two coaxial rollers. The presence of axis bending influences the magnitudes and the orientation of all forces (centrifugal, Coriolis and gravity).

2.3. Heat transfer and solidification

The assumption of a fully developed laminar flow of the liquid melt naturally dictates a parabolic velocity profile in the radial direction. Concerning the temperature evolution, the Prandtl number *Pr* is responsible for the delay between the fully developed velocity and temperature profiles. In this case, the thermal diffusion is stronger than viscous forces *(Pr*<1*)*; therefore, the flow can be treated as a thermally fully developed flow. According to Oosthuizen [15], temperature profile of thermally fully developed flow resembles the velocity profile. Therefore, the temperature profile is assumed to be parabolic as well. 2D average temperature field is obtained by solving the energy transport equation:

$$\frac{D}{Dt}\left(h\rho T\right) = \nabla\cdot\left(k\nabla T\right) + S_{T,l\to s}, \tag{5}$$

where k is the thermal conductivity and $S_{T,l\to s}$ is the heat source due to the heat conducted to the mould. Solidification is governed by coupling of the Stefan condition for the moving liquid-solid interface with the heat conduction to the mould. Since heat fluxes can be expected mainly in radial direction, only a 1D heat conduction equation is solved. It was derived in cylindrical coordinates for dimensionless space variable x^* defined by:

$$x^* = \frac{x - r(t)}{R_{ex} - r(t)}, \tag{6}$$

where x and $r(t)$ are distances of actual position and the moving interface from the mould axis, respectively. R_{ex} is the outer radius of the mould. Then, the heat conduction equation in the radial direction has the following form:

$$s(t)^2 \frac{\partial T}{\partial t} = \alpha \frac{\partial^2 T}{\partial x^{*2}} + \left(\frac{\alpha s(t)}{x^* s(t) + r(t)} + s(t)(x^* - 1)v \right) \frac{\partial T}{\partial x^*}, \quad (7)$$

where $s(t)=R_{ex}-r(t)$, α is thermal diffusivity. The velocity of moving interface, v, is determined by the 1D Stefan condition [16]:

$$\rho L v = \frac{k}{s(t)} \frac{\partial T}{\partial x^*}\bigg|_{x^*=0} - Q_{l \to s} + Q_{s \to a}, \quad (8)$$

where L is the latent heat. The first term on the right-hand side is the heat diffused into the solid shell. The second term signifies the heat flux from liquid to solid. The last term stands for the heat flux from liquid to air. From the physical point of view, this heat flux should be applied in equation (5); however, this naturally implies that solidification might start from the free liquid interface. It is expected that due to the density difference between liquid and solid all possible germens solidifying on the free surface will be centrifuged towards the mould wall. Therefore, the heat flux between liquid and air is applied in equation (8). Both equations (7) and (8) are one-dimensional, but are solved for each element of the 2D grid, on which the shallow water equations are solved. Heat transfer from free liquid surface to air is described by convective heat losses and radiation. Radiative heat transfer is further divided into heat redistribution inside the mould and heat losses via extremities. Losses due to the heat convection are defined as:

$$Q_{convection} = HTC_{\text{in}} (T_s - T_a), \quad (9)$$

where T_s and T_a are temperatures of the free liquid surface and air (323 K). HTC_{in} is the convective heat transfer coefficient. In the model it was set to a constant value of 100 $Wm^{-2}K^{-1}$. Radiative heat redistribution inside the mould is derived assuming the black body theory as follows:

$$Q_{rad,in} = f_x \sigma \varepsilon (T_s^4 - T_{avg}^4), \quad (10)$$

where f_x is the view factor depending on axial position (approximated using 4th degree polynomial) and σ and ε are the Stefan-Boltzmann constant and the emissivity (ε = 0), respectively. T_{avg} is the average temperature of free liquid interface given by:

$$T_{avg}^4 = \frac{\sum_{i=1}^{cells} f_{xi} T_s^4}{\sum_{i=1}^{cells} f_{xi}}, \quad (11)$$

Similarly, heat losses via extremities are:

$$Q_{rad,out} = (1 - f_x) \sigma \varepsilon (T_s^4 - T_a^4). \quad (12)$$

Similar relations are found for heat losses from the external mould wall. The convective HTC_{out} was set to a constant value of 150 $Wm^{-2}K^{-1}$. Temperature of air T_a is the same as in equation (9). Temperature of external mould wall is obtained from equation (7). Finally, radiative heat losses are calculated using equation (12) except that T_s is replaced with temperature of external mould wall and f_x is set to zero.

3. Results and discussion

The horizontal casting set-up is shown in Figure 2. The contour map represents the height of liquid metal after 3 s.

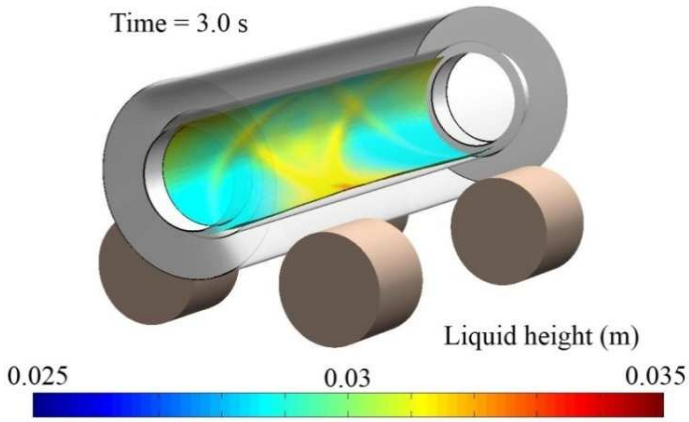

Figure 2. Liquid metal (height) distribution inside the mould.

Mould dimensions and material properties are listed in Table 1. Difference between external and internal radius of the mould gives the mould thickness (0.203 m). To keep the model simple and comprehensible all material properties are constant.

Table 1. Mould dimensions and material properties.

parameter	value (m)	property name	value
length of the mould	3.2	density	6800 kg/m^3
internal radius of the mould R_{in}	0.372	thermal conductivity	30 W/m-K
external radius of the mould R_{ex}	0.575	specific heat	750 J/kg-K
distance between two coaxial rollers λ	1.92	latent heat [a]	250 kJ/kg
axis bending A	0.002	dynamic viscosity	0.006 Pas

[a] used in Stefan condition only.

Several numerical cases were studied with varying initial liquid height h. Initial conditions can be summarized as follows: uniform distribution of liquid metal inside the mould, velocities set to zero, uniform temperature of the mould (433 K), temperature of free surface equal to the filling temperature (1755 K). Additionally, the mould is spinning at 633 rpm, which corresponds to an angular frequency Ω of 71.2 rad/s. The temperature of the liquid-solid interface is set to the liquidus temperature (1586 K).

For evaluation of results the internal mould wall was unfolded into a horizontal plane with x-axis and y-axis corresponding to axial and circumferential position, respectively. In Figure 3, the plot shows a snapshot of waves on the free surface of the melt spreading on already solidified shell. While the free surface evidently fluctuates, the liquid-solid interface remains smooth and nearly flat. The reason for that is due to the difference of characteristic times. The characteristic time of the flow can be defined as a reciprocal value of a wave frequency. It can be roughly estimated from the angular velocity Ω of the mould. It is approximately 0.1 s. The characteristic time of the solidification can be computed as the liquid height h divided by the solidification rate. Assuming the highest solidification rate occurring in the beginning (~0.01 m/s) the corresponding characteristic time is of the order of 1 s. The difference between characteristic times is thus at least one order of magnitude. In addition, the absence of the filling system and consequently the uniform temperature distribution along the internal mould wall also promotes uniform solidification.

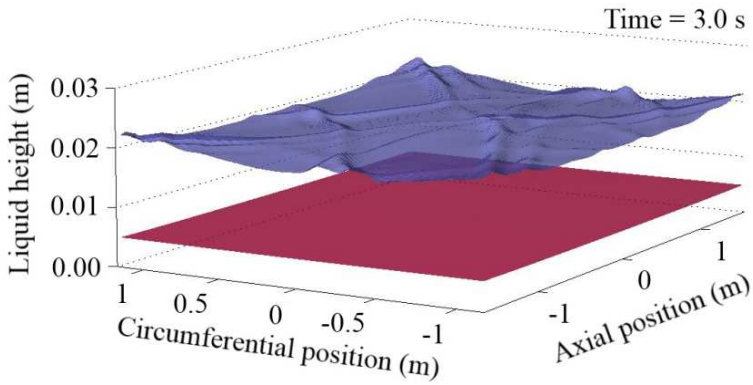

Figure 3. Waves travelling on free surface (blue) of melt with solid shell (red) beneath.

In Figure 4, transient temperature profiles are plotted in the radial direction for the case of the initial liquid height of 10 mm. The position of temperature record corresponds to the point (0, 0) in Figure 3. Dotted lines represent the corresponding parabolic temperature profiles in the liquid metal, while solid lines denote temperature profiles in both the solid metal and the mould. Only a small part of the mould close to the internal wall is depicted with coordinates ranging from 0 to 0.02 m. In the beginning, due to very high temperature gradient in the mould solidification is very fast (~0.01 m/s). However, due to heat conducted to the mould temperature gradient weakens and the solidification rate drops as time progresses. The solidification rate drops from more than 0.01 m/s below 0.001 m/s. In less than 10 s the melt is consumed and solidification is finished. Heat transfer however continues and temperature of the free surface further drops due to heat losses and heat conduction to the mould. Despite high temperatures inside the mould, a good thermal conductivity, and a perfect contact between the solid shell and the mould, temperatures of the outer part of the mould are still decreasing even after 25 s due to prevailing heat losses to air.

In Figure 5, three cases with different initial liquid heights (10, 20, and 30 mm) are compared. The data were recorded at the point (0, 0) (Figure 3). In the beginning, the heat conduction to the mould is so dominant that it leads to the same solidification rate for all three cases. Later on, curves diverge mainly because the solidification rate is also governed by the temperature gradient within the liquid metal. Markers indicate the end of solidification. It takes 85 s to solidify for the case of 30 mm of the melt height.

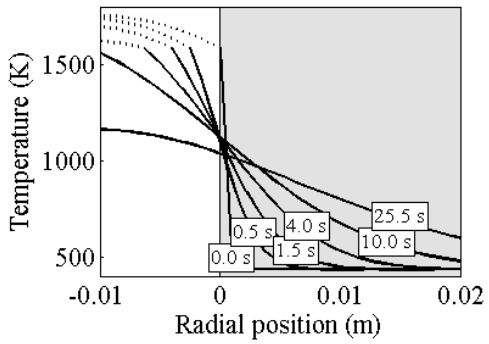

Figure 4. Typical temperature profiles in radial direction at different times; parabolic temperature profile inside the melt (dotted line) and computed temperature profile inside the solidified shell and the mould.

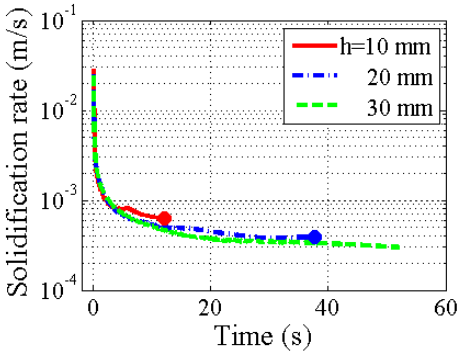

Figure 5. Solidification rate vs. time for different initial liquid heights (10, 20, and 30 mm); Markers signify end of solidification.

Solidification dynamics is naturally different from the mould centre to the extremities. Rate of solidification depends mainly on heat flux to the mould, but it is also influenced by heat flux from the liquid metal and heat losses from the free surface (Eq. 8). In Figure 6, contributions of each type of heat flux are compared in terms of temperature gradients plotted against time for the case for an initial liquid height 10 mm and without axis deformation.

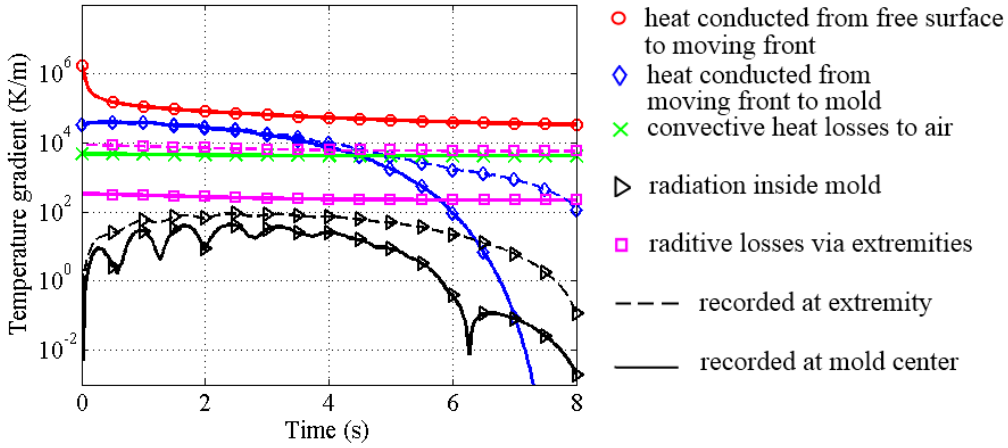

Figure 6. Temperature gradients as function of time.

Heat conduction from the moving interface to the solid (red circle) obviously dominates all other contributions during the whole process and is independent from the position in the mould. On the contrary, the radiative heat transfer inside the mould is the least dominant (black right-pointing triangle). The convective heat losses to air (green cross) are driven by the temperature of the free surface T_s. T_s almost does not depend on position in the mould because heat is mainly transported by the flow. This implies convective heat losses to air are independent of position. During the solidification, the free surface temperature T_s varies only from the initial temperature (1755 K) to the liquidus temperature (1586 K). Therefore, convective heat losses to air do not vary much in time. Radiative heat losses through extremities (magenta square) are nearly unchanged, but they decrease significantly from the mould extremity to the mould centre. Separation of curves (blue diamond) representing heat conduction in the liquid reflects a higher solidification rate near mould extremities.

4. Conclusions and future prospects

A numerical model of horizontal centrifugal casting of work roll has been developed based on the shallow water equations for multi-layer system. Flow dynamics is solved in the tangential and the axial direction considering flow variables averaged along the liquid height. The heat conduction in the radial direction was coupled with the Stefan condition for the moving liquid-solid interface. The mould deformation or more specifically, the deformation of the mould centreline was considered. Further, vibrations were introduced by perturbation of gravity.

Several simulations were conducted to study the flow dynamics of the liquid melt, wave patterns of the free surface, solidification. Results show wave propagation on the free surface. Wave amplitudes grow with increasing height of liquid metal. In the beginning of each simulation a single longitudinal wave was developed due to the counteracting of gravity and inertia forces. Later on, it was scattered into other longitudinal waves with smaller amplitudes. A lifetime of longitudinal waves was dependent on the amplitude of the axis bending. Generally, the higher the bending, the faster the transition to a developed flow regime. If there were only longitudinal (or horizontal) waves, the flow dynamics would not provide sufficient mixing in the axial direction which would most likely led to uneven microstructure along the mould length. On the other hand, in the tangential direction the mixing would be contrarily very strong. Purely annular waves would rather result in a uniform temperature field of the liquid metal. In the conducted simulations, neither longitudinal nor annular waves were observed

in the developed flow regime. The waves were generally propagating in transversal direction, smoothing out temperature variations and thus, promoting a uniform solidification represented by a flat moving front. As the solidification proceeded, viscous forces became dominant and free surface fluctuations were lowered gradually. While the free surface was dynamically distorted by travelling waves, the liquid-solid interface remained smooth and nearly flat. Solidification rate was higher at extremities than in the mould centre due to higher radiative heat losses. Radiative heat transfer inside the mould was found to have only a negligible effect on solidification. Effect of vibrations was found to be negligible. The final solidified shell was however naturally influenced by the axis bending. The thickness of the shell varied along both, the tangential and the axial direction.

The current model is still under development and it is still to be extended to account for the moving mushy zone by using an extra layer with variable viscosity. Mould filling is also an important phenomenon and will be included. Further, thermal resistance due to mould coating and a possible air gap caused by shrinkage of the shell has to be included.

Acknowledgement
This work is financially supported by the Materials Center Leoben and the Eisenwerk Sulzau–Werfen.

References

[1] Chirita G, Stefanuscu I, Barbosa J, Puga H, Soares D and Silva F S 2009 On assessment of processing variables in vertical centrifugal casting technique *Int. J. of Cast Metals Research* **22** 382–9
[2] Keerthiprasad K S, Murali M S, Mukunda P G and Majumdar S 2010 Analysis of fluid flow in centrifugal casting, *Front. Mater. Sci. China* **4** 103–10
[3] Chirita G, Stefanuscu I, Soares D and Silva F S 2006 Centrifugal versus gravity casting techniques over mechanical properties, *Anales de Mecánica de la Fractura* **1** 317–22
[4] Keerthiprasad K S, Murali M S, Mukunda P G and Majumdar S 2010 Numerical simulation and cold modeling experiments on centrifugal casting, *Metall.Mater. Trans. B* **42** 144–55
[5] Zagórski R and Śleziona J 2007 Pouring mold during centrifugal casting process, *Archives of Materials Science and Engineering* **28** 441-4
[6] Raju P S S and Mehrotra S P 2000 Mathematical modelling of centrifugal casting of metal matrix composites, *Material Transactions JIM* **41** 1626–35
[7] Drenchev L, Sobczak J, Malinoc S and Sha W 2003 Numerical simulation of macrostructure formation in centrifugal casting of particle reinforced metal matrix composites. Part 1: model desription, *Modelling Simul. Mater. Sci. Eng.* **11** 635–49
[8] Pedlosky J 1987 *Geophysical Fluid Dynamics* (New York: Springer-Verlag)
[9] Knauss J A 1996 *Introduction to Physical Oceanography* (New Jersey: Prentice Hall)
[10] Dellar P J and Salmon R 2005 Shallow water equations with a complete Coriolis force and topography, *Phys. of Fluids* **17** 1-23
[11] Saint-Venant A J C 1871 Théorie du movement non permanent des eaux, avec application aux crues de rivieres et a l'introduction des marrees dans leur lit, *C. R. Acad. Sc. Paris* **73** 147-54
[12] Bohacek J, Kharicha A, Ludwig A and Wu M 2011 Liquid metal inside a horizontally rotating cylinder under vibrations, *Proc. Int. Conf. Experimental Fluid Mechanics* vol 2 (Liberec) pp 564-73
[13] Bohacek J, Kharicha A, Ludwig A and Wu M 2011 Shallow water equations for a liquid film in horizontally rotating cylinder, *Proc. Int. Conf. Computational Mechanics* (Pilsen)
[14] Martinez G, Garnier M and Durand F 1987 Stirring phenomena in centrifugal casting of pipes, *Applied Scientific Research* **44** 225–39
[15] Oosthuizen P and Naylor D 1999 Introduction to Convective Heat Transfer Analysis *(Boston: WCB/McGraw-Hill)*
[16] Dantzig J A and Rappaz M 2009 Solidification *(Lausanne: EPFL Press)*